

Custom Transient Finite Element for the Modelling of Ultrasonic Control Methods for Downhole Well Integrity

Jordan Barras^{*1}, Nicolas Leymarie¹, Delphine Landois¹, Alexandre Imperiale¹, Edouard Demaldent¹, Philippe Bredif¹, Orland Guedes², Hiroshi Hori², Roel Van Os²

¹ Université Paris-Saclay, CEA-List, Palaiseau, France

²SLB – Études et Productions Schlumberger, Clamart, France

*corresponding author, E-mail: jordan.barras@cea.fr

Abstract

The transient spectral element method can be understood as a specific high-order finite element method that is particularly accurate and fast with a low memory footprint, hence enabling 3D ultrasonic testing simulations on a standard PC. However, particular care must be taken in its settings when seeking both practicality and performance. In comparison, fast semi-analytical simulation using ray tracing is easily accessible to nondestructive testing experts, through the CIVA simulation software. Although this approximate model effectively deals with a wide range of industrial applications, it reaches its limits in certain cases, particularly at relatively low frequencies involving resonance phenomena. To deal with these challenging inspection configurations, CEA-List is working on dedicated finite element models in the CIVA framework to meet specific needs in a compromise between efficiency and accuracy.

The case study considered in partnership with SLB perfectly illustrates the benefits of developing such a modelling approach. SLB provides cased-well imaging services using ultrasonic resonance methods to evaluate oil and gas well integrity. Defective cased wells have irregularities, such as corroded casings with pitting, localized cement debonding and channelings. Simulated ultrasonic signals of the actual wells are useful to understand the measurements and are available by finite element modelling with sufficient accuracy. However, the associated computational costs for numerous model cases limit the building of the model database as the digital twin of the actual well logging.

The development strategy of dedicated hybrid finite element applications adopted by CEA-List is presented in broad outline. Cross-model comparisons on a reference configuration of pristine cases are presented, highlighting the effective limits of standard CIVA ray models. The contribution offered by the new hybrid finite element approach is then discussed. We discuss the evolution of model functionalities to handle geometries that differ from the canonical case (interface defects, loss of thickness in

arbitrary geometries, etc.) from the perspective of a digital twin of this control.

1. Introduction

Ultrasonic measurements are one of the nondestructive testing (NDT) methods used with oil and gas well tubulars to ensure the safe hydrocarbon production from subsurface reservoirs. Ultrasonic transducers are deployed downhole to evaluate the thickness of tubulars and acoustic impedance (AI) of material outside the tubulars, respectively for tubular corrosion and well cement quality evaluation. The transducers excite wide-band frequency signals below 1 MHz to excite signals near the fundamental thickness resonance of tubulars in acoustically attenuative downhole environment.

Semi-analytical methods are very popular in the NDT industry thanks to relatively low calculation times compared to finite element methods (FEM).

This is the case of the models implemented in the CIVA platform: CIVA-UT provides an accurate estimation of the ultrasonic field radiated by an ultrasonic transducer in a propagation media that can be fluidic, elastic or a combination of several materials in a structure of which geometries are much larger than the elastic wavelength, which is often the case in the NDT industry.

The semi-analytic modelling software URAI, developed at SLB, uses a similar approach in terms of transducer signal modelling, but is based on an analytical elastic response of a cylindrically layered structure to a very wide band excitation. Near the frequency of the fundamental thickness mode resonance of the tubular, strong compressional and shear-coupled modes are excited. This coupling invalidates the CIVA software model that uncouples the longitudinal and the transversal calculations. A simulation of the cylindrical geometry has been carried out by CIVA-UT as a test, and it shows such a discrepancy in the results.

One of the limits of the URAI model appears when the geometry of the inspected part is not a cylinder, includes a defect or exhibits some other irregularity. In this case the formulation of the analytical elastic response is insufficient.



The main way to accurately simulate such geometries is in the use of FEM software, such as OnScale. Calculation times, however, are much higher than those for semi-analytic methods.

One of the strengths of the CIVA software lies in the combination of several models to solve the ultrasonic propagation. One of them is using standard CIVA-UT models in a wide propagation zone, combined with a finite element domain that is defined only around a zone of interest, here the elastic cylinder. The result is a compromise between a shorter calculation time offered by the CIVA-UT module and the accuracy of the FEM zone. In the current commercial version of CIVA, only a defect can be included in the FEM area. In the method described in this paper, this principle has been extended, such that the part itself can be included.

2. Evaluation of the well integrity

In the past decades, the oil & gas industry has invested considerably in the well integrity domain. One of the key aspects is to provide a good cement quality behind a steel casing that ensures the sealing of hydrocarbons from the reservoirs to the different zones of the well.

SLB offers a solution involving ultrasonic technology to evaluate the acoustic impedance behind a steel casing [1] [2] [3]. A commercial downhole ultrasonic imager uses an ultrasonic transducer mounted on a rotor that enables an azimuthal scan from the interior of a well. Such tool is deployed downhole at the end of a logging cable to transmit measured data while running into or pulling out of a well. The transducer is excited at the central frequency of 500 kHz and the received signal is processed using the T^3 algorithm [1] dedicated to obtaining the thickness of the casing and the acoustic impedance behind the casing in real time.

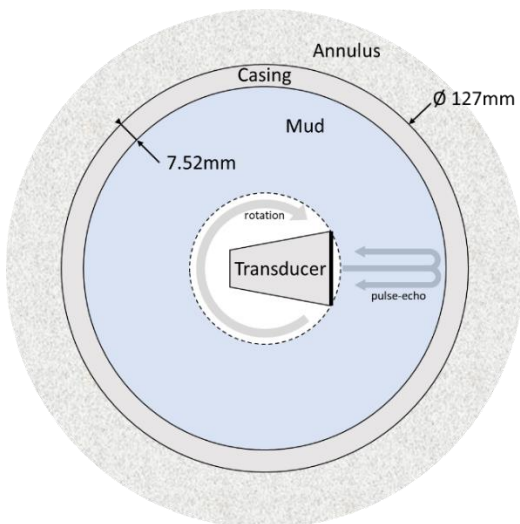


Figure 1: Ultrasonic signal simulation in a water-filled casing surrounded by annular material.

3. State of the art of simulation tools for the SLB case study

Figure 1 shows a schematized cross-section of a wellbore with a single casing. The fluid inside the casing is often referred to as ‘mud’. The casing itself is typically made of carbon-steel. The annular space behind the casing is typically filled with a cement.

The acoustic impedance of material behind casing may vary in the range from about 0 to 10 MRayl, respectively from gas to high-density well cement. Table 1 shows three typical materials to be discriminated during the control that is simulated for this case study. If cement is compromised in quality, inclusions or entire connected paths of water or gas may be present in the cement. The downhole ultrasonic imager can distinguish between the different acoustic impedances and discriminate cement from water and gas. As such, it provides a response of the integrity of the cement.

Table 1: Material parameters of the annulus

Material	V_L	V_T	ρ	Z_L
	(m/s)	(m/s)	(g/cm ³)	(MRayls)
Water	1500	/	1.01	1.52
Cement 1	3600	2000	1.90	6.84
Cement 2	3000	1600	1.70	5.10

3.1. Simulation using URAI

The model used by SLB is based on the resolution of acoustic wave scattering through reciprocity relations. These developments led to the simulation of the response of ultrasonic transducers interacting with fluid-loaded cylindrically layered elastic structures [4] [5] [6].

3.2. Simulation using OnScale FEM

The modelling of ultrasonic wave-propagation is well defined by finite element codes. In this study, OnScale [7] is used to provide reference FEM results. The code uses an explicit scheme that allows a parallelization of the calculation. The OnScale platform sends the tasks to cloud computing servers to speed up the computation process.

3.3. Simulation using CIVA

The computation of ultrasonic fields and inspections in CIVA is performed with two different models.

The first one, implemented in the historical CIVA-UT module, is a semi-analytic and under high-frequency assumption formulation [8] of the main bulk waves usually interfering in the NDT applications (namely longitudinal and transverse waves in the solids). A relatively restricted number of interactions with the specimen boundary is computed, taking into account all possible wave conversions. Defects of dimension above the wavelength can also be treated through analytic diffraction models or more generically by FEM boxes englobing the defect [9]. A custom CIVA module, that is currently under development, integrates an in-house finite element solver

that relies on transient spectral element method (SEM). The latter is usually coupled to the semi-analytical model, which sets the loading source on well-chosen coupling boundaries. The resolution is performed following a domain decomposition approach: the topology of the scene is described by a macro mesh that allows solving separately an acoustic problem in fluid zones and an elastodynamic problem in solid zones. The transfer conditions between two neighboring macro elements are realized by mortar elements [10]. The high-order micro mesh, which is used for the SEM computation, is generated automatically according to the considered minimum wavelength.

4. Dedicated hybrid simulation chain

A fully integrated simulation procedure is set in place. It begins with the specimen generation, done by a built-in plugin implemented in C++ and Python. Parameters that define the nominal casing are controlled with a dedicated graphical interface (see Figure 2). This interface can be completed in the future to describe damaged casings. The FEM mesh is automatically generated. Then, the specimen can be used either for CIVA-UT or for hybrid simulations. This framework is not specific to the actual study case and can be easily derived for other applications [11].

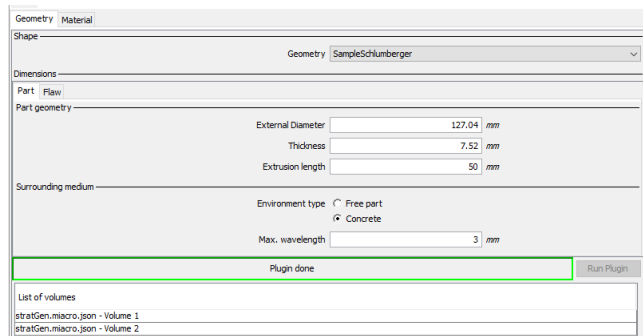


Figure 2. View of the specimen generation plugin graphical user interface.

4.1. Calibration procedure

The calibration part is a simple steel tube with an external diameter of 139.7 mm and a thickness of 2 mm. It is filled with water and the inspection is done, in immersion, on the internal surface. The external surface is left free.

The macro mesh of the complete specimen is thus a triple ring extruded along its axis. The three layers are the part itself, a fluid layer and a fluid perfectly matched layer (PML) that is settled in the inner side (see Figure 3).

The CIVA user starts by defining a region of interest (ROI) in the CAD view provided by the specimen generator plugin. Such region has a geometry surrounding the piece or solely the coupling region, with a part in the mud. The ROI is meshed, and the calculation is performed with the boundary conditions defined above.

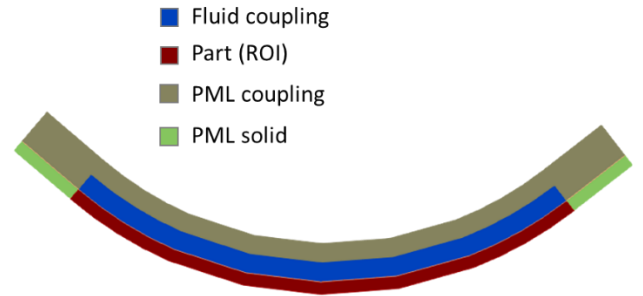


Figure 3. Macro scene of a calibration configuration using the ROI subdivision.

To be able to quantitatively compare the simulation with the experimental measurements, a calibration procedure is deployed based on the measurement of the experimental A-Scan $V^{(cal)}$ obtained with the calibration part.

Because of the resonant character of this configuration, a simple calibration on the amplitude gain is not sufficient. The objective is to obtain the reference signal $s^{(ref)}$ which, if used as an excitation signal during the simulation, returns the experimental A-Scan on the calibration part. We thus have:

$$\underline{V}^{(cal)}(\omega) = \underline{H}^{(cal)}(\omega) \cdot \underline{s}^{(ref)}(\omega), \quad (1)$$

where $\underline{H}^{(cal)}$ is the simulated transfer function. To obtain the reference signal, it is first necessary to characterize this transfer function over the frequency band over which $V^{(cal)}$ is non-zero. This is done by performing a first simulation, denoted by (0), on the calibration part and taking an excitation signal $s^{(0)}$ whose spectrum encompasses the target bandwidth of the probe. We can summarize this simulation by writing:

$$\underline{V}^{(0)}(\omega) = \underline{H}^{(cal)}(\omega) \cdot \underline{s}^{(0)}(\omega). \quad (2)$$

Hence the term $\underline{H}^{(cal)}$ can be made to disappear by dividing the two previous equalities member by member. The reference signal is expressed as a function of the experimental A-Scan measured on the calibration part and the preliminary simulation data as:

$$\underline{s}^{(ref)}(\omega) = \frac{\underline{V}^{(cal)}(\omega)}{\underline{V}^{(0)}(\omega)} \cdot \underline{s}^{(0)}(\omega). \quad (3)$$

Finally, the introduction of a factor $\epsilon \ll 1$ regularizes the spectral division for near zero values of $\underline{V}^{(0)}$:

$$s^{(ref)}(t) = \mathcal{F}^{-1} \left(\frac{\underline{V}^{(cal)} \cdot (\underline{V}^{(0)})^*}{|\underline{V}^{(0)}|^{2+\epsilon}} \cdot \underline{s}^{(0)} \right) (t). \quad (4)$$

This calibration procedure uses a rather basic deconvolution method of the experimental calibration signal. Its implementation has been done using a web app framework integrated in this custom CIVA version (see Figure 4) providing the new reference signal to use in the .civa file of the preliminary simulation.

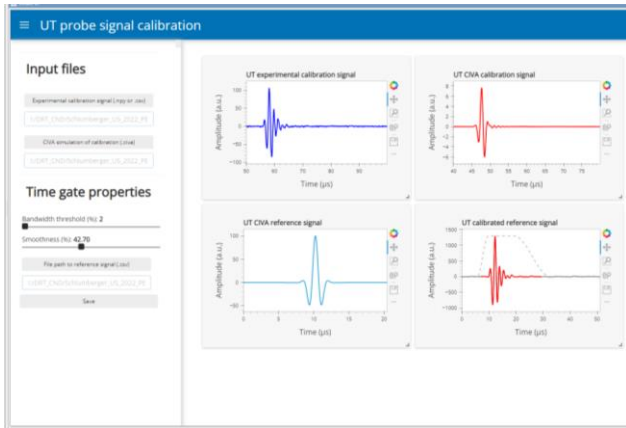


Figure 4. Graphic user interface of the calibration app.

To verify the correct operation of the procedure, we compare the experimental A-Scan with the simulated A-Scan obtained from this calibrated reference signal. According to Figure 5, we observe a very good agreement, except for the noise filtering. The calibration procedure thus meets the specifications.

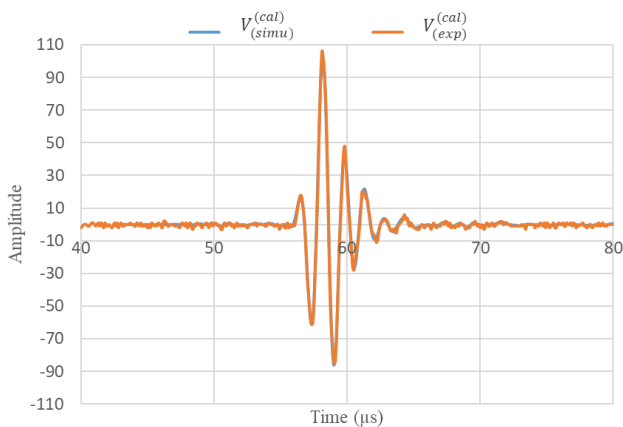


Figure 5. Validation of the calibration procedure by reproducing the experimental signal, using the reference signal as an input to the calibration simulation.

4.2. Simulation of a casing

Now we aim to model the situation presented in Figure 1. The difference with the calibration specimen is that the metallic tube does not have free outer boundary conditions. Instead, a cement layer must be added. Wave reflections at the outer cement radius are not of interest to the current simulation. Therefore, only a thin cement layer needs to be meshed (~ 1 or 2 wavelengths) and surrounded by a solid PML. The ROI can still be applied, as shown in Figure 6.

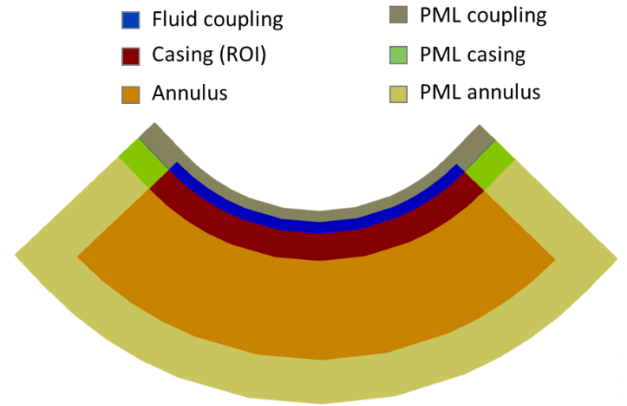


Figure 6. Macro scene of a casing configuration using the ROI subdivision.

5. Results and Discussion

Four modeled time-domain signals from the aforementioned methods are presented in Figure 7. The signals are bandpass-filtered in 400 ± 50 kHz frequency range and scaled to better visualize the match among the four simulations.

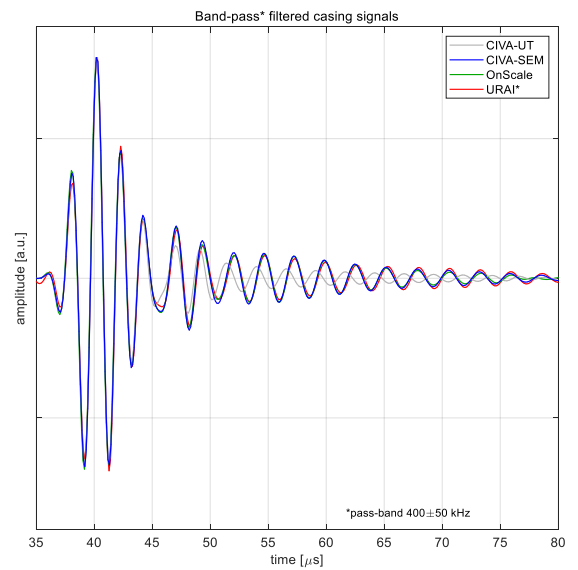


Figure 7: Simulated time-domain signals, 400 ± 50 kHz bandpass-filtered.

The signals are inverted to the casing thickness and annular AI using T^2 processing excluding the correction for nonplanar geometry [1]. Inverted AI and casing thickness values are presented in comparison to the model input AI values, respectively in Figure 8 and Figure 9. Figure 9 presents the inverted resonance frequencies, normalized by a reference frequency, i.e., inverse two-way traveling time of the compressional wave in casing thickness. The resonant frequency is negligibly dependent on annular impedance. Relatively large deviation of CIVA-UT results from other models indicates its limited applicability to

simulation of the casing resonance in this example case. Indeed, CIVA-UT is a propagation model that is not designed to deal with resonance problems (contrarily to the URAI model) and is usually applied to more classical bulk waves inspections.

6. Conclusions

After the confirmation that the CIVA-UT module was not adapted for low-frequency well inspection, a dedicated semi-analytic / FEM simulation tool is implemented. Every useful option is accessible using the CIVA graphical user interface. A simple and easy-to-use frequency calibration method is also made accessible using an add-in framework. Results of the hybrid method are compared with results from a commercial FEM code and with results from the URAI analytical model. It confirms the validity of the proposed dedicated tool.

Further developments will consist of adding reference defects as supplementary options of the specimen generator plugin and to study their influence on the extracted acoustic impedance. Such defects include canonic holes made on purpose to qualify the inspection method with the calibration part. Finally, the goal is to detect and characterize real defects, in particular thickness losses due to corrosion, channeling in the cement layer and so-called micro-annuli (thin fluid or gas inclusions between the metallic casing that hamper the interpretation of the cement integrity).

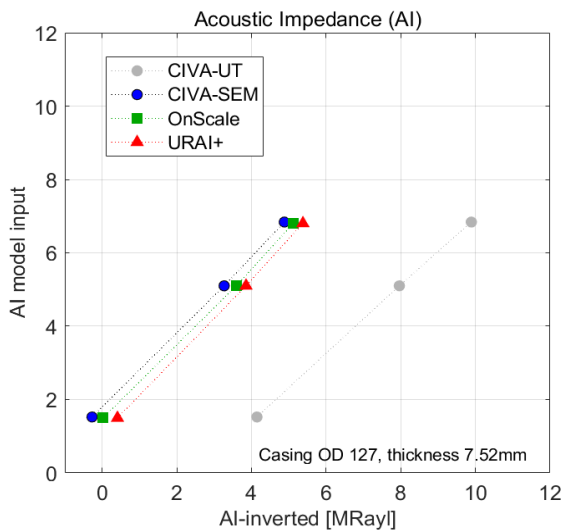


Figure 8: Inverted annular acoustic impedance.

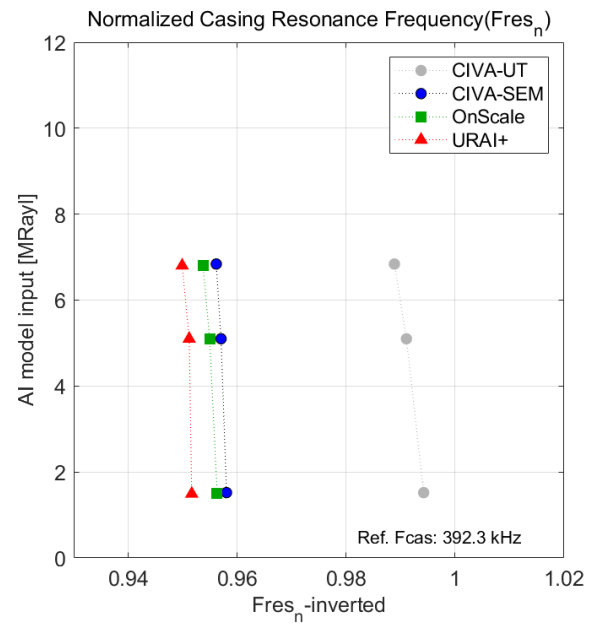


Figure 9: Estimated normalized casing resonance frequency.

7. References

- [1] A. Hayman, R. Hutin and P. Wright, "High Resolution Cementation and Corrosion Imaging by Ultrasound," in *SPWLA 32nd Annual Logging Symposium*, June 1991.
- [2] R. Van Kuijk, S. Zeroug, B. Froelich, M. Allouche, S. Bose, D. Miller, J.-L. Le Calvez, V. Schoepf and A. Pagnin, "A Novel Ultrasonic Cased-Hole Imager for Enhanced Cement Evaluation," in *International Petroleum Technology Conference*, Doha, Qatar, November 2005.
- [3] S. Thierry, C. Klieber, M. Lemarenko, J.-L. Le Calvez, T. Brill, T. Barrou, A. Hayman, F. Mege and R. Van Os, "New-Generation Ultrasonic Measurements for Quantitative Cement Evaluation in Heavy Muds and Thick-Wall Casings," in *SPE Annual Technical Conference and Exhibition*, Dubai, UAE, September 2016.
- [4] C. Randall and F. Stanke, "Mathematical model for internal ultrasonic inspection of cylindrically layered structures," *The Journal of the Acoustical Society of America*, vol. 83, no. 4, pp. 1295-1305, April 1988.
- [5] S. Zeroug, F. Stanke and R. Burrige, "A Complex-Transducer-Point Model for Finite Emitting and Receiving Ultrasonic Transducers," *Wave Motion*, vol. 24, pp. 21-40, 1996.
- [6] S. Zeroug, "Spectral Integral Formulae for the Response of Acoustic Transducers in Cylindrically Curved Configurations," *IEEE Transactions on*

- Ultrasonics, Ferroelectrics and Frequency Control*, vol. 45, no. 3, pp. 768-778, May 1998.
- [7] OnScale, "Simulation of Ultrasonic Borehole Imaging," 14 January 2019. [Online]. Available: <https://spectrum.ieee.org/simulation-of-ultrasonic-borehole-imaging>. [Accessed February 2023].
- [8] N. Gengembre and A. Lhémy, "Pencil Method in Elastodynamics: Application to Ultrasonic Field Computation," *Ultrasonics*, vol. 38, no. 1, pp. 495-499, March 2000.
- [9] A. Imperiale, N. Leymarie, T. Fortuna and E. Demaldent, "Coupling Strategies Between Asymptotic and Numerical Models with Application to Ultrasonic Non-Destructive Testing of Surface Flaws," *Journal of Theoretical and Computational Acoustics*, vol. 27, no. 2, p. 1850052, June 2019.
- [10] A. Imperiale and E. Demaldent, "A macro-element strategy based upon spectral finite elements and mortar elements for transient wave propagation modeling. Application to ultrasonic testing of laminate composite materials," *International Journal for Numerical Methods in Engineering*, vol. 119, no. 10, pp. 964-990, September 2019.
- [11] E. Demaldent, A. Imperiale, N. Leymarie and T. Fortuna, "Custom Transient Finite Element Method and Ray Tracing Hybridization Strategies for Ultrasonic Testing Modelling," in *13th ECNDT*, Lisbon, Portugal, July 2023.